American Journal of Condensed Matter Physics 2020, 10(2): 31-38
DOI: 10.5923/j.ajcmp.20201002.01

First Principles Studies of $Ca_xSr_{1-x}F_2$ Ternary Alloys

A. B. Olanipekun

Department of Pure and Applied Physics, Caleb University, Imota, Lagos, Nigeria

Abstract The structural and electronic properties of fluorite structures CaF_2, SrF_2 and their ternary alloy $Ca_xSr_{1-x}F_2$ for concentrations x = 0.25, 0.50, 0.75 are studied using first principles calculation. The pseudopotential plane-wave (PPPW) method as used in the QUANTUM ESPRESSO code is applied. In this method, the generalized gradient approximation (GGA) is employed for the exchange-correlation (XC) potential. The lattice constants a_0 and bulk modulus B, for CaF_2, SrF_2 and their ternary alloy $Ca_xSr_{1-x}F_2$ compounds were first carried out, followed by the band gap energies calculation of the binary fluorides and the ternary alloys. In order to correct the huge underestimation of DFT(GGA) method, a model involving the generalized gradient approximation method of Perdew, Burke and Ernzerhof (PBE) is used for the calculation of the band gap and a good agreement with experiment is obtained for the binary compounds with little deviation. The electronic band structures and the density of states of the alloys are presented.

Keywords Electronic properties, Structural properties, Generalized Gradient Approximation, Fluorite structures, Vergard's law

1. Introduction

The alkaline earth fluorides have been highly studied by first principles methods [1,2]. Both CaF_2 and SrF_2 are ionic insulators with a wide band gap. The Alkaline Earth Fluorides (AEF) have wide band gaps and low refractive indices. AEF find applications in optical coatings and transmissive components in the deep ultraviolet [3].

The electronic and ionic conductivity studies of fluorite type compounds (CaF_2, SrF_2, BaF_2 and $SrCl_2$) have been performed [4,5]. Calculation on ground state and lattice dynamical properties of ionic conductors CaF_2, SrF_2 and BaF_2 using density functional have been carried out [6,7]. Cadelano and Cappellini [8] in 2011 studied the electronic structure of CaF_2, SrF_2, BaF_2, CdF_2, HgF_2, PbF_2 by means of density functional theory within the local density approximation for the exchange correlation energy.

The ground state properties and electronic band structures of CaF_2, SrF_2 and CdF_2 have been calculated using the shell model in the pair potential approximation [9].

Structural stability of CaF_2 under high pressure was conducted using first-principles calculations based on density functional theory. The sequence of the pressure-induced phase transition of CaF_2 is the fluorite structure -*Fm*3*m*, the $PbCl_2$ type structure-*Pnma*, and the Ni_2In-type structure-$P6_3$ /mmc [10].

Phase transitions and equations of state of the alkaline earth fluorides CaF_2 and SrF_2 are examined up to 95GPa by angle-dispersive x-ray diffraction experiments in laser-heated diamond anvil cells at beamlines. They confirmed that both materials undergo a phase transition from the cubic fluorite structure to the orthorhombic cotunnite-type structure at pressures less than 10GPa. Both materials further transform to a hexagonal Ni_2In-type structure at 84 and 36GPa, respectively, following laser heating [11].

Hao and his coworkers showed using first-principles calculation based on density functional theory (DFT) with the plane wave basis set as implemented in the CASTEP code the phase transition of SrF_2 from the fluorite structure (*Fm*3*m*) to the $PbCl_2$-type structure (*Pnma*), and to the Ni_2In-type phase (*P*63/*mmc*) [12].

The sequence of pressure-induced phase transition of BaF_2 was simulated by using an atomistic calculation based on the shell model. This fluorite crystal presents two pressure-induced phase transitions at approximately 3 and 15GPa. At 3GPa, the fluorite phase transforms into the α-phase, which has an orthorhombic cotunnite-type structure ($PbCl_2$, Z = 4). At 15GPa, it transforms into hexagonal Ni_2In-type structure (*P*63/mmc, Z = 2) [13].

Liu and his co-workers extensively explored the structural and electronic properties of CdF_2 to high pressure by ab initio calculations based on the density functional theory [14]. PbF_2 has been shown to exist in the cubic, orthorhombic, hexagonal, and monoclinic phases [15].

It has been found that the complete phase-transition sequence for CoF_2 is tetragonal rutile ($P4_2$/mnm) ⟶ $CaCl_2$ type (orthorhombic Pnnm) ⟶ distorted PdF_2 (orthorhombic *Pbca*) + PdF_2 (cubic Pa-3) in coexistence ⟶ fluorite (cubic

* Corresponding author:
bukkymatt4real@yahoo.com (A. B. Olanipekun)
Received: Sep. 8, 2020; Accepted: Sep. 26, 2020; Published: Oct. 15, 2020
Published online at http://journal.sapub.org/ajcmp

*Fm*3*m*) ⟶ cotunnite (orthorhombic Pnma) [16]. Stavrou and his colleagues showed that MnF_2 exists in these structural phases; rutile, SrI_2 and $PbCl_2$ [17].

Hoat et al. reported first principles calculations of structural, electronic and optical properties of SrF_2 such as reflectivity, refraction index, conductivity and energy loss function under pressure, done using full-potential linearized augmented plane wave (FP-LAPW) method based on density functional theory as implemented on WIEN2k code [18].

Cappellini et al. investigated the electronic and optical properties of the stable clusters of alkaline earth metal fluorides, which include, MgF_2, CaF_2, SrF_2, and BaF_2 using density functional theory (DFT) and time-dependent DFT (TDDFT) methodss with a localized Gaussian basis set [19].

$Ca_xSr_{1-x}F_2$ is used as optical and laser materials [20]. $Ca_xSr_{1-x}F_2$ is applicable as an encapsulant or masking material for GaAs [21]. The alloy is also used in quantum devices e.g Resonant Tunneling Diodes [22].

Siskos et al. investigated the epitaxial growth of fluoride heterostructure of $Ca_xSr_{1-x}F_2/CdF_2/Ca_xSr_{1-x}F_2$ on Ge for quantum devices [21].

Klimma and his colleagues used the Czochralski method to grow $Ca_xSr_{1-x}F_2$ [23].

Oshita and his coauthors used the two-step growth method to grow $Ca_xSr_{1-x}F_2/CdF_2/$ $Ca_xSr_{1-x}F_2$ quantum well structure on Ge substrate [22].

Takahashi and Tsutsui in 2013 proposed the introduction of a SrF_2 buffer layer to $Ca_xSr_{1-x}F_2$ at x=0.42, i.e, $Ca_{0.42}Sr_{0.58}F_2/SrF_2$/Ge structure as a method for the growth of an electron-tunneling barrier layer on Ge with low leakage current [24].

In 2019, Suzuki et al. studied experimentally the band gap energy of $Ca_xSr_{1-x}F_2$ by changing the composition ratio of CaF_2 and SrF_2 and used the alloy to fabricate filterless vacuum ultraviolet photodetectors with wavelengths dependent on the band gap of the alloy [25].

The theoretical study of the electronic and structural properties of $Ca_xSr_{1-x}F_2$ composing of CaF_2 and SrF_2 are still not clear very well. In this work, we present a systematic study of the electronic and structural properties of $Ca_xSr_{1-x}F_2$ alloys in the fluorite-cubic structure.

2. Computational Method

First-principles calculations are performed to study the electronic and structural properties of $Ca_xSr_{1-x}F_2$ by employing a Ultrasoft pseudopotential [26] plane wave approach based on density functional theory (DFT) [27,28] and implemented in Quantum Espresso [29] code. The exchange-correlation contribution is described within generalized gradient approximation based on Perdew and Wang [30]. The orbitals of Ca ($3s^23p^64s^2$), Sr ($4s^24p^64d^15s^1$) and F ($2s^22p^5$) are treated as valence electrons. The k integration over the Brillouin zone is performed using the Monkhorst and Pack mesh [31]. A mesh of six special k-points was taken in the Brillouin zone for the binary compounds and for the alloys. The total energy of the crystal converged to less than 1mRyd after seven iterations A 6x6x6 sampling k point is utilised for the calculation of the total energy of the fluorite crystals. The lattice constants and bulk moduli are fitted to the total energy and volume to the Murnaghan's equation of state [32], it allows to get the equilibrium structural properties of both the binary and ternary compounds.

As a starting point, we calculated the structural properties of the binary compounds CaF_2 and SrF_2 in the fluorite phase using GGA scheme. The ternary alloys in cubic fluorite structure are modelled at some selected compositions of x and are described by periodically repeated supercells.

3. Results and Discussion

3.1. Structural Properties

For the binary fluorides and their alloys, the lattice parameter and the bulk modulus are determined. The alloys were studied by using a primitive mesh of 12 atoms. The values obtained for different compositions of Ca for the lattice parameters and bulk modulus are given in Table 1 and 2 respectively. The calculated properties are in good agreement with experiments and theoretical results for the binary compounds. The lattice constant decreases with concentration, x. The calculated values of the bulk modulus, using the GGA approximation, decreases from CaF_2 to SrF_2; from the lower to the higher atomic number. This suggests that SrF_2 is more compressible than CaF_2. The variation of the lattice parameter and bulk modulus as a function of the concentration of alloy $Ca_xSr_{1-x}F_2$ is illustrated by Figure 1 and Figure 2, respectively. We note that the lattice parameter decreases almost linearly as a function of the concentration. Our calculations deviate from those calculated by Vegard's law [33]

$$a_{AB_{1-x}C_x} = (1-x)a_{AB} + xa_{AC} \quad (1)$$

where a_{AB}, a_{BC} and $a_{AB_{1-x}C_x}$ are the lattice parameters of binary compounds AB, AC and ternary alloy $AB_{1-x}C_x$ respectively. However, the linear behaviour is not followed by many alloys and a general form is expressed by a semi-empirical quadratic relationship [34,35]. Hence, the lattice constant can be written as:

$$a_{AB_{1-x}C_x} = (1-x)a_{AB} + xa_{AC} - x(1-x)b \quad (2)$$

where the quadratic term b is the bowing parameter. For the ternary alloy, (2) can be rewritten as

$$a_{Ca_xSr1-xF2} = (1-x)a_{CaF2} + xa_{SrF2} - x(1-x)b \quad (3)$$

We compared calculated lattice parameters with those obtained from Vergard's Law at different x. There is a marginal downward bowing of 0.064Å due to smaller size of Calcium (Ca) atom (than that of Strontium (Sr).

Figure 2 shows the bulk modulus as a function of Ca-composition x for $Ca_xSr_{1-x}F_2$ compounds. B increases with composition x. The quadratic fit to the bulk modulus is

given as

$$B_{Ca_xSr1-xF2} = (1-x)B_{CaF2} + xB_{SrF2} - x(1-x)b \quad (4)$$

Table 1. Calculated Lattice Parameters, a(Å) of $Ca_xSr_{1-x}F_2$

Composition, x	Present work	Others	Experiment
1	5.479	5.30[i]	5.46[ii]
0.75	5.576		
0.50	5.664		
0/25	5.743		
0	5.816	5.68[i]	5.80[ii]

[i]Ref [41] – LDA/PAW
[ii]Ref [42]

Table 2. Calculated Bulk modulus, B(GPa) of the $Ca_xSr_{1-x}F_2$

Composition, x	Present work	Others	Experiment
1	83.0	103.01[i]	82.71[iii]
0.75	78.7		
0.50	75.5		
0/25	73.2		
0	70.7	83.75[i]	69.0[iv]

[iii]Ref [43]
[iv]Ref [1]

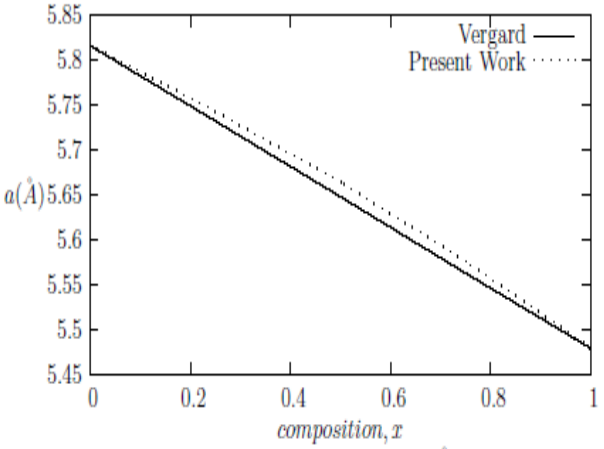

Figure 1. Variation of lattice parameters, a(Å) of $Ca_xSr_{1-x}F_2$ with composition, x

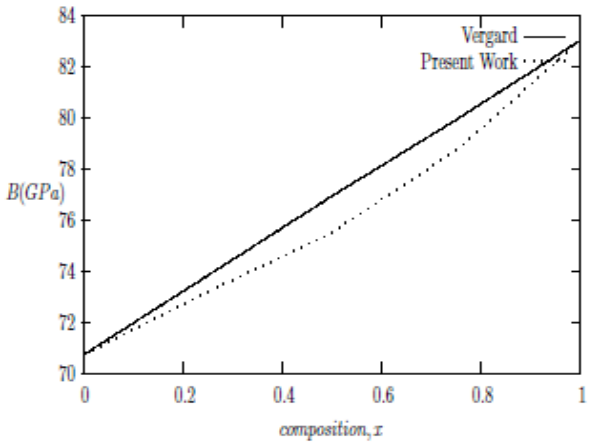

Figure 2. Variation of Bulk Modulus, B of $Ca_xSr_{1-x}F_2$ with composition, x

There is a small deviation from the linear concentration dependence (LCD) in the Bulk Modulus, which gives a slight downward bowing of 5.07GPa with the quadratic fit. The small bowing parameter is due to the bulk modulus of SrF_2 which is 14.82% smaller than CaF_2.

3.2. Electronic Properties

From the GGA scheme, the band-gaps of the ternary alloys and the corresponding binary compounds are presented in Table 3. Energy band gaps are computed along the high symmetry points and compared with experiments as well as available theoretical results. The discrepancy seen in the table is an intrinsic feature of DFT. The calculated band gap is 30-40% less than experiment [36-38]. However, it is accepted that electronic band structures from GGA calculations are qualitatively in good agreement with experiments regarding the ordering of energy levels and band shapes [39]. There is a direct gap at Gamma point in all the ternary alloys.

Table 3. Calculated Band gap energy, Eg(eV) of $Ca_xSr_{1-x}F_2$

Composition, x	Present work	Others	Experiment
1	7.347	7.43[i]	11.80[v]
0.75	7.148		
0.50	7.048		
0/25	7.012		
0	6.942	6.89[i]	10.60[v]

[v]Ref [44]

Table 4. DFT(PBE) and empirical model calculated band gap energy, E_g(eV) of $Ca_xSr_{1-x}F_2$

Composition, x	DFT(PBE)	Model
1	7.43	10.98
0.75	7.23	10.71
0.50	7.14	10.59
0/25	7.10	10.54
0	7.03	10.44

The band gap can be improved by using the empirical model of Morales-García, et al. for semiconductors and insulators [40]. From the model, the band gap energy is derived to be:

$$E_g(model) = 1.355284E_g\ (PBE) + 0.916192 \quad (5)$$

The band gaps of the binary fluorides and their alloys are also calculated using the generalized gradient approximation method of Perdew, Burke and Ernzerhof (PBE). The band gaps of the binary compounds obtained using the empirical model compare well with experiment. The $Ca_xSr_{1-x}F_2$ alloys are wide gap insulators.

Energy bands structures for various concentrations of Calcium are shown in Figures 3, 4 and 5. For the alloy, the band structures for all concentrations of Ca gave a direct gap at the Γ point. The band gap energy is the difference between the valence band maximum and conduction band minimum.

The composition dependence of $Ca_xSr_{1-x}F_2$ band-gaps

over the composition range (0-1) can be well fitted by the following expression,

$$Eg_{Ca_xSr1-xF2} = (1-x)Eg_{CaF2} + xEg_{SrF2} - x(1-x)b \quad (6)$$

where $Eg_{Ca_xSr1-xF2}$ denotes the band gap energy of $Ca_xSr_{1-x}F_2$, Eg_{CaF2} and Eg_{SrF2} signify the band gap energy of CaF_2 and SrF_2, respectively while b is the band gap bowing parameter of $Ca_xSr_{1-x}F_2$.

Figure 6 shows that the direct gap versus concentration, exhibit a non-linear behavior. The direct gap exhibits a downward bowing with a mean value of 0.345eV within the range of x investigated. The fundamental gap increases considerably with the Calcium composition, x.

The variation of the band gap bowing in $Ca_xSr_{1-x}F_2$ with concentration is shown in Figure 7. The bowing remains linear and increases with calcium concentration.

Figures 8, 9 and 10 show the partial density of states of Ca, Sr and F respectively. The red line represents s-orbitals, green line represents p-orbitals and blue line represents d-orbitals. Ca and Sr contain s, p and d orbitals while F contains only s and p orbitals. The partial density of states of the constituent elements of the alloys are used to analyze the total density of states of the alloys.

The total DOS for the ternary alloys, $Ca_xSr_{1-x}F_2$ are depicted in Figures 11 and 12 at x=0.25 and 0.50 respectively. The DOS for these concentrations are very similar but the values of the peaks are different according to the composition. There are five regions. The peak at the lowest energy states, which is due to the s electrons of the fluorine, while the next two regions contain the contribution of Ca-s and Sr-s orbitals respectively. The region just below the Fermi level E_F is predominately p states of F, with only a small contribution for p-Ca and p-Sr states. Above the Fermi level, the region is predominately p states of Ca and p and d states of Sr.

The total DOS for the ternary alloy $Ca_xSr_{1-x}F_2$ is given in Figure 13 for the concentration x = 0.75. We observed four regions. The first region at the lowest energy states, is due to the s electrons of the fluorine, while the next region contains the contribution of Ca-s and Sr-s orbitals. The region just below the Fermi level E_F is predominately p states of F, with only a small contribution for p-Ca and p-Sr states. Just above the Fermi level, the region is predominately p states of Ca and p and d states of Sr.

From the DOS plots, as Ca composition increases in the alloys, the density of states of Ca-s and Ca-p orbitals decrease while the density of states of Ca-d orbitals increase. The DOS of s orbital of F increase with Ca concentration in all the alloys while that of p orbitals decrease. The DOS of s, p and d orbitals of Sr decrease with Ca composition in the alloys.

The DOS for the different concentrations of all alloys indicate that the band contributions of Ca-s, Ca-p, Sr-s, Sr-p, Sr-d, and F-p orbitals gradually weaken with Ca composition but Ca-d and F-s orbitals contributions strengthen.

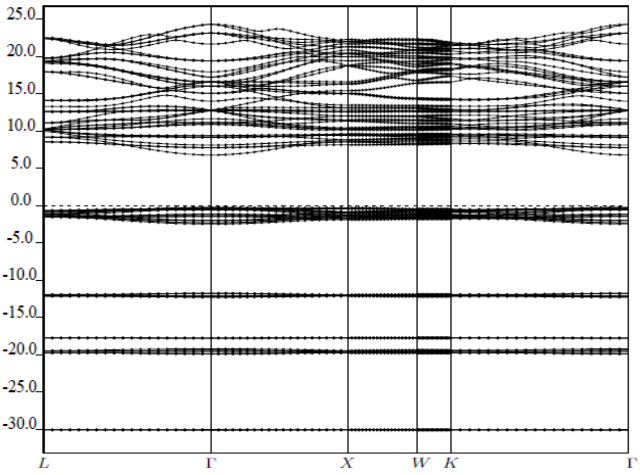

Figure 3. Electronic band structure of $Ca_{0.25}Sr_{0.75}F_2$ alloy

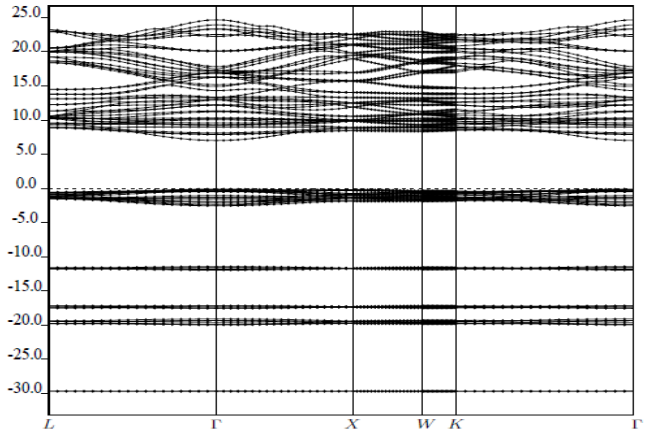

Figure 4. Electronic band structure of $Ca_{0.50}Sr_{0.50}F_2$ alloy

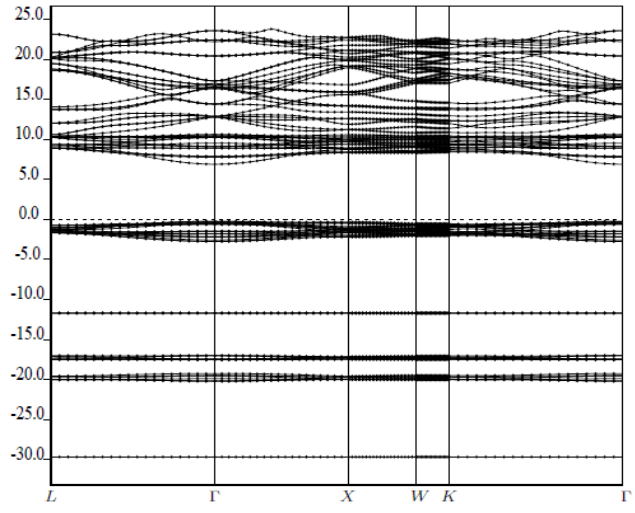

Figure 5. Electronic band structure of $Ca_{0.75}Sr_{0.25}F_2$ alloy

For Figures 3-5, vertical axis represents Energy (eV) while horizontal axis represents wave vector, k.

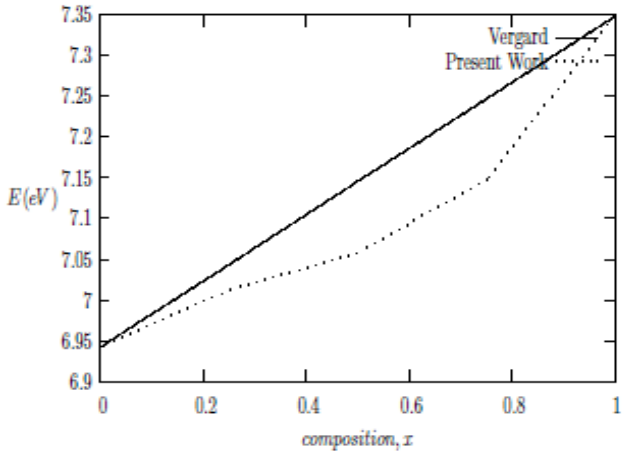

Figure 6. Variation of Band Gap Energy of $Ca_xSr_{1-x}F_2$ with composition, x

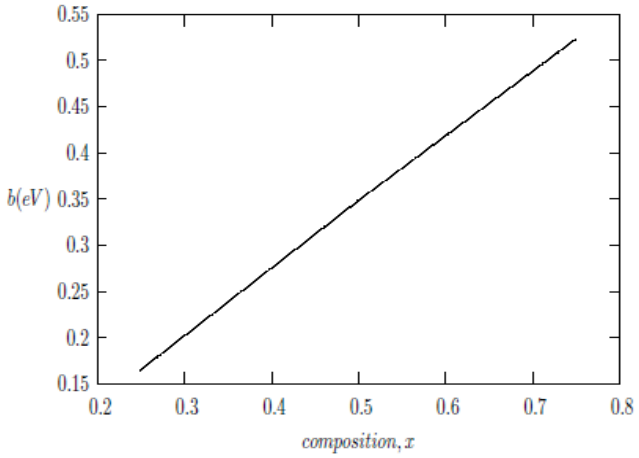

Figure 7. Variation of band gap bowing parameters, b(eV) of $Ca_xSr_{1-x}F_2$ with composition, x

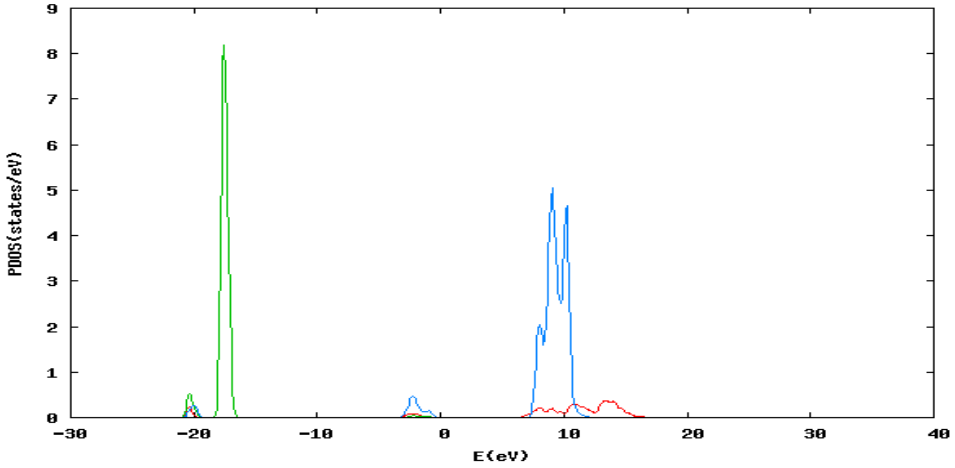

Figure 8. Partial density of states (PDOS) of Calcium (Ca)
red line represents s-orbitals
green line represents p-orbitals
blue line represents d-orbitals

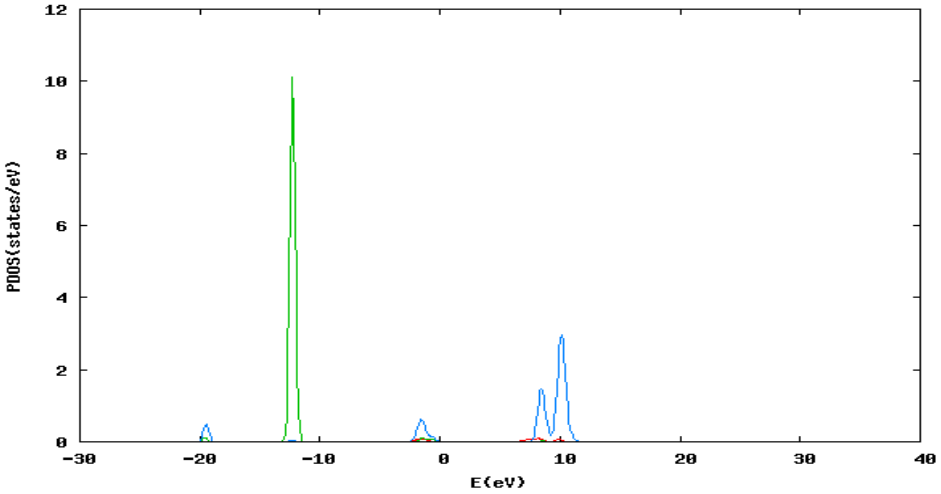

Figure 9. Partial density of states (PDOS) of Strontium (Sr)
red line represents s-orbitals
green line represents p-orbitals
blue line represents d-orbitals

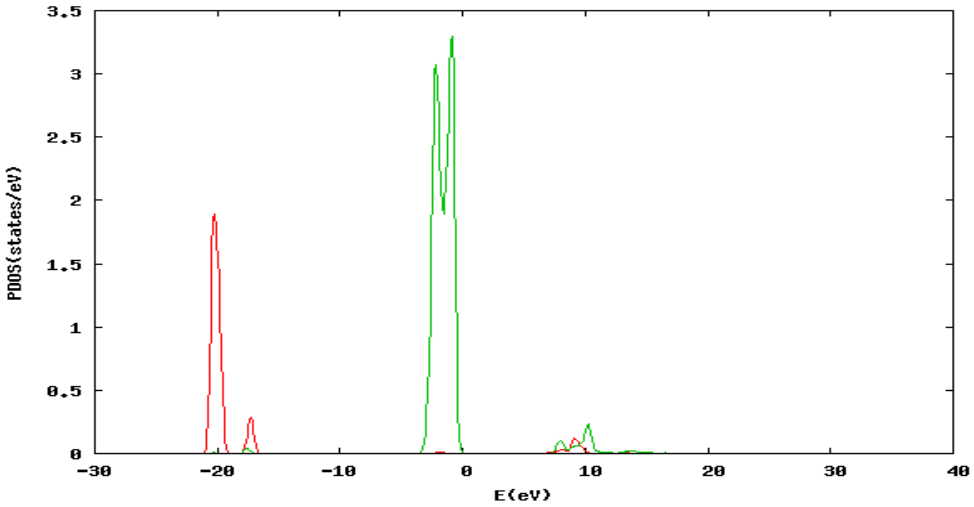

Figure 10. Partial density of states (PDOS) of Fluorine (F)
red line represents s-orbitals
green line represents p-orbitals

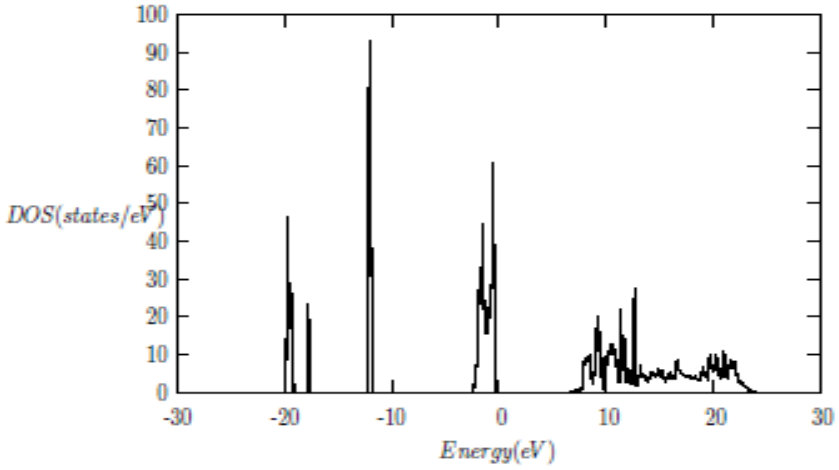

Figure 11. Calculated total density of states (DOS) of $Ca_{0.25}Sr_{0.75}F_2$

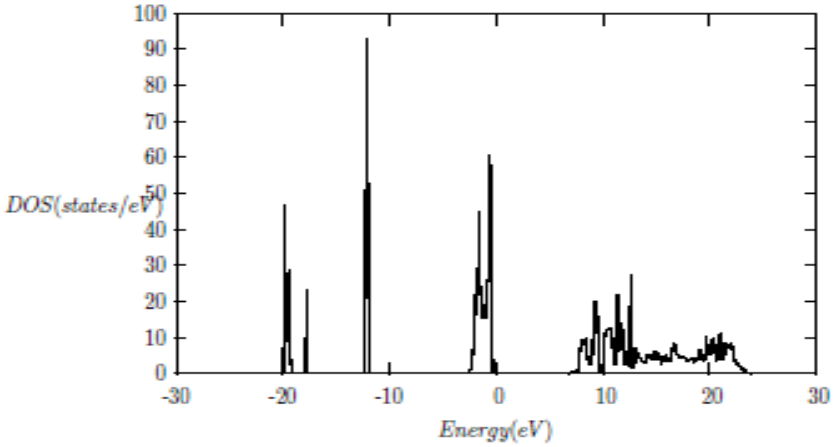

Figure 12. Calculated total density of states (DOS) of $Ca_{0.50}Sr_{0.50}F_2$

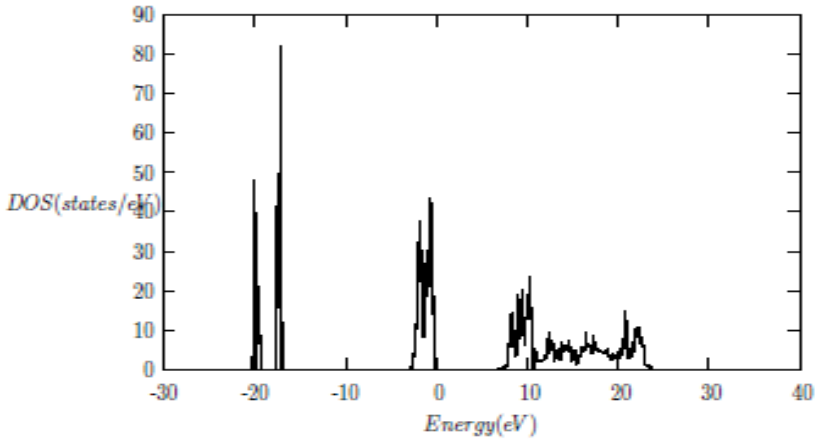

Figure 13. Calculated total density of states (DOS) of $Ca_{0.75}Sr_{0.25}F_2$

4. Conclusions

The PP-PW method within the GGA approximations have been used to investigate the structural and electronic properties of the cubic $Ca_xSr_{1-x}F_2$ alloys. We have calculated the equilibrium lattice constants and bulk moduli of the binary compounds and the alloys. For the purpose of comparison, the structural properties of the binary compounds of the alloys were calculated. Good agreement is found between our calculations and experiments. The bowings of the lattice constant, bulk modulus and energy band gap are also investigated. From the graph of lattice constant and bulk modulus against composition, x, the values of the structural properties can be predicted at any desired concentration, x. The $Ca_xSr_{1-x}F_2$ alloys for the composition x = 0.25, 0.50 and 0.75 are wide gap insulators and may be a good material for optoelectronic industry. Their calculated band gap energies showed that all the alloys can absorb the short wavelength Ultraviolet (UV) light and hence can find application in the UV metal-insulator-semiconductor light emitting diodes.

REFERENCES

[1] Samara, G.A. 1976. Temperature and pressure dependence of the dielectric properties of alkaline-earth fluorides. Phys. Rev. B 13: 4529-4544.

[2] Hazen, R.M. and Finger, L.W. 1981. Optical and lattice dynamical properties of simple ionic crystals. J. Appl. Crystallography 14: 234-245.

[3] Song, K.S. and Williams, R.T. 1993. Alkaline Earth Fluorides. Solid-State Sciences 105: 96-122.

[4] Evarestov, R.A., Murin, I.V. and Petrov, A.V. 1989. Electronic structure of fluorite-type crystals. J. Phys. Condens. Matt. 1: 6603-6609.

[5] Voronin, B.M. and Volkoy, S. 2001. Ionic conductivity of fluorite type crystals CaF_2, SrF_2, BaF_2, and $SrCl_2$ at high temperatures. J. Phys. and Chem. of Solids 62:1349-1358.

[6] Soni, S., Gupta, S.K., Talati, M. and Jha, P.K. 2011. The ground state and lattice dynamical study of ionic conductors CaF_2, SrF_2 and BaF_2 using density functional theory. Physica B Condens. Matt. 72: 934-939.

[7] Schmalzl, K. 2007. Volume and pressure dependence of ground-state and lattice-dynamical properties of BaF_2 from density-functional methods. Phys. Rev. 75: 014306-014312.

[8] Cadelano, E. and Cappellini, G. 2011. Electronic structure of fluorides: general trends for ground and excited state properties. Eur. Phys. J. 81: 115-120.

[9] Nikiforov, A.I., Yakimov, A.I., Duarechenskii, S.A. and Chaikovskii, S.V. 2002. Barrier height and Tunneling current in Schottky diodes with embedded layers of quantum dots. J. Experimental and Theoretical Physics Letters 75: 102-106.

[10] Wu, X., Qin, S. and Wu, Z. 2006. First-principles study of structural stabilities, and electronic and optical properties of CaF_2 under high pressure. Phys. Rev. B73: 134103-134110.

[11] Dorfman, S. M., Jiang, F., Mao, Z., Kubo, A., Prakapenka, V. and Duffy, T. S. 2010. Phase transitions and equations of state of alkaline earth fluorides CaF_2, SrF_2, and BaF_2 to Mbar pressures. Phys. Rev. B 81: 174121-174129.

[12] Hao A., Yang, X., Li, J., Xin, W., Zhang, S., Zhang, H. X. and Liu, R. 2009, First-Principles Study of Structural Stabilities, Electronic and Optical Properties of SrF_2 under High Pressure. Chin. Phys. Lett. 26: 077103-077106.

[13] Jiang, H., Pandey, R., Darrigan, C. and Rerat, M. 2003. First-principles study of structural, electronic and optical properties of BaF_2 in its cubic, orthorhombic and hexagonal phases. J. Phys.: Condens. Matter 15: 709–718.

[14] Liu, G., Wang, H., Ma, Y. and Ma, Y. 2011, Phase transition of cadmium fluoride under high pressure. Solid State Communications 151: 1899-1902.

[15] Costales, A., Blanco, M.A., Pandey, R. and Recio, J.M. 2000. Theoretical characterization of the high-pressure phases of PbF_2. Phys. Rev. B61: 359-362.

[16] Barreda-Argueso, J.A., Lopez-Moreno,S., Sanz-Ortiz, M.N., Aguado, F., Valiente,H., Gonzalez,J., Rodrıguez, F., Romero, A.H., Munoz, A., Nataf, L. and Baudelet, F. 2013. Pressure-induced phase-transition sequence in CoF_2: An experimental and first-principles study on the crystal, vibrational, and electronic properties. Phys. Rev. B88:

214108-214122.

[17] Stavrou, E., Yao, Y., Goncharov, A., Konopkova, Z. and Raptis, C. 2015. High-pressure X-ray diffraction, Raman, and computational studies of MnF_2. Phys. Rev. B93: 054101-054108.

[18] Hoat, D.M., Rivas Silva, J.F., M´endez Blas, A. and R´ıos R´amirez, J.J. 2018. Effect of pressure on structural, electronic and optical properties of SrF_2: A first principles study. Revista Mexicana de Fisica 64: 94-100.

[19] Cappellini, G., Bosin, A., Serra, G., Furthmüller, J., Bechstedt, F. and Botti, S. 2020. Electronic and Optical Properties of Small Metal Fluoride Clusters. ACS Omega 22: 13268–13277.

[20] Kaminskii, A., Mikaelyan, R. and Zygler, I. 1969. Spectral investigation of the stimulated radiation of Nd^{3+} in CaF_2-YF_3. Physical Status Solidi B 31: 85-86.

[21] Siskos, S., Fountaine, C. and Munoz-Yague, A. 1984. Epitaxial growth of lattice-matched $Ca_xSr_{1-x}F_2$ on (100) and (110) GaAs substrates. J. Appl. Phys. 56: 1642-1646.

[22] Oshita, T., Takahashi, K. and Tsutsui, K. 2009. Growth of ultra-thin fluoride heterostructures on Ge(111) for quantum devices. J. Crystal Growth. 311: 2224-2226.

[23] Klimma, D. Rabe, M. Bertrama, R. Uecker, R. and Parthier, L. 2008. Phase diagram analysis and crystal growth of solid solutions $Ca_{1-x}Sr_xF_2$. J. Crystal Growth 310: 152-155.

[24] Takahashi, K. and Tsutsui, K. 2013. Growth of Thin Epitaxial $Ca_xSr_{1-x}F_2/SrF_2$ Layers with Low Leakage Current on Ge Substrate. Japanese J. Appl. Phys. 5: 100203-100207.

[25] Suzuki, K., Cadatal-Raduban, M., Kase, M. and Ono, S. 2019. Band gap engineering of $Ca_xSr_{1-x}F_2$ and its application as filterless vacuum ultraviolet photodetectors with controllable spectra responses. Optical Materials 88: 576-579.

[26] Furthmuller, J., Kachell, P. and Bechstedt, F. 2000. Extreme softening of Vander-bilt pseudopotentials. Physical Review B 61: 4576-4587.

[27] Hohenberg, H. and Kohn, W. (1964), Inhomogenous electron gas. Phys. Rev. B136: 864-871.

[28] Kohn, W., and Sham, L.J. 1965. Self-consistent equations including exchange and correlation effects. Phys. Rev. A 140: 1133-1138.

[29] Giannozzi, P., Baroni, S., Bonini, N., Calandra, M., Car, R., Cavazzoni, C., Ceresoli, D., Chiarotti, G.L., Cococcioni, M., Dabo, I., Corso, A.D., de Gironcoli, S., Fabris, S., Fratesi, G., Gebauer, R., Gerstmann, U., Gougoussis, C., Kokalj, A., Lazzeri, M., Martin-Samos, L., Marzari, N., Mauri, F., Mazzarello, R., Paolini, S., Pasquarello, A., Paulatto, L., Sbraccia, C., Scandolo, S., Sclauzero, G., Seitsonen, A.P., Smogunov, A., Umari, P. and Wentzcovitch, R.M. 2009. QUANTUM RESSO: a modular and open-source software project for quantum simulations of materials. J. Phys. 21: 395502-395520.

[30] Perdew, J. and Wang, Y. 1992. Accurate and simple analytic representation of the electron-gas correlation energy. Phys. Rev. B 45: 13244-13252.

[31] Monkhorst, H.J., Pack, J.D., 1976. Special points for Brillouin-zone integrations. Phys. Rev. B 13: 5188-5192.

[32] Murnaghan, F. D. 1944. The Compressibility of Media under Extreme Pressures. Proceedings of the National Academy of Sciences of the United States of America 30: 244-247.

[33] Vegard, L. 1921. The constitution of mixed crystals and the space occupied by atoms. Zeitschrift fur Physik B: Condensed Matter 5: 17-26.

[34] El Haj Hassan, F. and Akbarzadeh, H. 2006, First-principles elastic and bonding properties of barium chalcogenides. Comput. Mater. Sci. 35: 423-445.

[35] El Haj Hassan, F., Hashemifar, S.J. and Akbarzadeh, H. 2006. Density functional study of $Zn_{1-x}Mg_xSe_yTe_{1-y}$ Quaternary semiconductor alloys. Phys. Rev. B73: 195-202.

[36] Fahy, S., Chang, K.J., Louis, S.G. and Cohen, M.L. 1989. Pressure coefficients of band gaps of diamond. Phys. Rev. B 39: 7840-7847.

[37] Bachelet, G.B. and Christensen, N.E. 1995. Relativistic and core relaxation effects on the energy bands of GaAs and Ge. Physical Review B 31: 879-887.

[38] Onida, G., Reining, L. and Rubio, A. 2002. Electronic excitations: density-functional versus many-body Greens-function approaches. Rev. Mod. Phys.74: 601-659.

[39] Boukhris, N., Meradji, H., Ghemid, S., Drablia, S. and Hassan, F.E.H. 2011. Ab initio study of the structural, electronic and thermodynamic properties of $PbSe_{1-x}S_x$, $PbSe_{1-x}Te_x$ and $PbS_{1-x}Te_x$ ternary alloys. Phys. Scr. 83: 065701-065709.

[40] Morales-García, A., Valero, R. and Illas, F. 2017. An empirical, yet practical way to predict the band gap in solids by using density functional band structure calculations. J. Phys. Chem. 121: 18862-18866.

[41] Cadelano, E. and Cappellini, G. 2011. Electronic structure of fluorides: general trends for ground and excited state properties. Eur. Phys. J. 81: 115-120.

[42] West, A.R. 1999. Basic Solid State Chemistry. John Wiley and Sons, Chichester, England. 126pp.

[43] Weast, R.C. 1976. Chemical Rubber Company Handbook of Chemistry and Physics, CRC Press, Boca Raton, Florida, United States. 2390pp.

[44] Rubloff, G.W. 1972. Far-Ultraviolet Reflectance Spectra and the Electronic Structure of Ionic Crystals. Phys. Rev. B 5: 662-684.